

Beyond broadband: towards a spectral decomposition of EEG microstates

Victor Férat¹, Martin Seeber¹, Christoph M. Michel^{1,2}, Tomas Ros^{1,2}

¹ Functional Brain Mapping Laboratory, Department of Basic Neurosciences, Campus Biotech, University of Geneva, Geneva, Switzerland

² Centre for Biomedical Imaging (CIBM) Lausanne-Geneva, Geneva, Switzerland

Keywords: EEG ; microstates; topography; Resting state ; eyes closed ; eyes open ; alpha; mutual information

Highlights:

- Microstate topographies are similar across standard EEG bands.
- The temporal dynamics of microstate topographies are independent across standard EEG bands
- Band-specific microstate analysis may reveal more specific and/or novel effects compared to broadband microstate analysis

Abstract

Microstate (MS) analysis takes advantage of the electroencephalogram's (EEG) high temporal resolution to segment the brain's electrical potentials into a temporal sequence of scalp topographies. Originally applied to alpha oscillations in the 1970s, MS analysis has since been used to decompose mainly broadband EEG signals (e.g. 1-40 Hz). We

29 hypothesized that MS decomposition within separate, narrow
30 frequency bands could provide more fine-grained information
31 for capturing the spatio-temporal complexity of multichannel
32 EEG. In this study using a large open-access dataset (n=203),
33 we pre-filtered EEG recordings into 4 classical frequency bands
34 (delta, theta, alpha, beta) in order to compare their individual
35 MS segmentations using mutual information as well as
36 traditional MS measures. Firstly, we confirmed that MS
37 topographies were spatially equivalent across all frequencies,
38 matching the canonical broadband maps (A, B, C, and D).
39 Interestingly however, we observed strong informational
40 independence of MS temporal sequences between spectral
41 bands, together with significant divergence in traditional MS
42 measures (e.g. mean duration, time coverage). For instance, MS
43 sequences in the alpha-band exhibited temporal independence
44 from sequences in all other frequencies, whilst also being
45 longer on average (>100 ms). Based on a frequency vs. map
46 taxonomy (e.g. θA , αC , βB), narrow-band MS analyses revealed
47 novel relationships that were not evident from the coarse-
48 grained broadband analysis. Overall, our findings demonstrate
49 the value and validity of spectral MS analysis for decomposing
50 the full-band EEG into a richer palette of frequency-specific
51 microstates. This could prove useful for identifying new neural
52 mechanisms in fundamental research and/or for biomarker
53 discovery in clinical populations.

54

55

56 **1 Introduction**

57 Multi-channel Electroencephalography (EEG) is a long-established tool for
58 exploring the human brain’s spatio-temporal activities. Microstate (MS)
59 analysis [1] , first introduced by Lehmann [2] in 1971, takes advantage of
60 EEG’s high temporal resolution to segment EEG signals into short
61 successive periods of time characterized by metastable scalp
62 topographies. Initially applied to narrow-band alpha oscillations (8 -12
63 Hz)[2], microstate analysis is nowadays usually performed on broadband
64 EEG signals (1 – 40Hz) [1], [3]. Historically, only a limited number of
65 studies [4]–[6] have focused on applying MS analysis to the traditional
66 frequencies associated with cortical oscillations (e.g. delta, theta, alpha,
67 beta etc.). For example, in the 1990’s, Merrin et al [4] were the first to
68 report on a significant difference in MS segments between schizophrenic
69 patients and controls specifically in the theta EEG band. On the other hand,
70 more recent work in healthy subjects found that MS dynamics were
71 independent of EEG power fluctuations across the frequency spectrum [7],
72 which technically supported the rationale for performing broadband MS
73 analysis. Neuroimaging studies have nevertheless emerged showing that
74 anatomically-distinct cortical regions display different dominant EEG
75 frequencies, with occipito-parietal regions more active in the alpha band,
76 and prefrontal regions being biased more toward delta or theta power
77 [8]–[10]. Moreover, ongoing cortical dynamics have been reported to
78 fluctuate from a local resting/idling alpha oscillatory state to task-specific
79 active mode(s) dominated by other rhythms (e.g. theta [11], gamma [12]
80). As a consequence, cortical regions could combine different frequencies
81 for integrating/segregating information across large-scale networks, a
82 phenomenon termed “oscillatory multiplexing” [13]. Finally, of more
83 clinical significance, a growing body of work has indicated abnormal EEG

84 spectral power in distinct frequencies across cortical regions in a variety
85 of brain disorders [14], [15]. Therefore, given that different spatial
86 topographies uncovered by MS analysis imply anatomically-distinct
87 cortical generators (according to the forward-model of EEG generation
88 [1]), it is reasonable to hypothesize that distinct MS topographies may
89 display different spatial and/or temporal profiles across the frequency
90 spectrum.

91 To investigate this question as well as gain a deeper understanding of
92 frequency-specific MS signature(s), we sought to explicitly decompose MS
93 spatio-temporal dynamics within *discrete, narrow-band frequency bands*
94 (i.e. delta, theta, alpha, and beta), with the aim of comparing them to the
95 classical analysis of the broadband signal.

96 Here, we employed a validated, open-source dataset [16] of resting-
97 state EEG recordings from 203 healthy subjects during both eyes opened
98 and eyes closed conditions. These were then filtered in the classical EEG
99 bands (delta: 0-4 Hz, theta: 4-8 Hz, alpha: 8-12 Hz, beta: 15-30 Hz) to
100 obtain band specific signals. These narrow-band signals, in addition to the
101 broadband (1-30 Hz) signal, were then independently subjected to
102 standard microstate analysis [17]. Map topography, mean duration,
103 occurrence, time coverage, and global explained variance (GEV) were used
104 as quantitative measures of spatiotemporal microstate dynamics. In
105 summary, and using spatial correlation analysis, we firstly demonstrate
106 remarkably similar microstate topographies across frequencies, closely
107 matching the classical broadband maps. Interestingly, however, we
108 observed strong informational independence of microstate sequences
109 between frequencies, in addition to significant differences in established
110 measures of temporal dynamics (mean duration, occurrence, and time
111 coverage).

112 In conclusion, our results support a more diverse, frequency-specific
113 application of microstate analysis compatible with the narrow-band MS
114 analyses of early pioneers [2], [4]. We anticipate this approach to provide
115 a more fine-grained spectral information not visible to the standard
116 broadband analysis, for example in the identification of biomarkers in
117 clinical populations or for understanding the mechanisms underlying EEG
118 microstates.

119 **2 Methods**

120 **2.1 Dataset**

121 EEG recordings were obtained from 203 anonymized participants
122 enrolled in the Mind-Brain-Body study [16]. Detailed protocol and
123 inclusion criteria are reported in [16]. The overall sample consisted of 227
124 participants divided into 2 groups: the younger adults group with
125 participant age ranging between 20 and 35 years ($N = 153$, 45 females,
126 mean age = 25.1 years, $SD = 3.1$) and an older adults group with age
127 ranging between 59 and 77 years ($N = 74$, 37 females, mean age = 67.6
128 years, $SD = 4.7$). Medical and psychological screening was conducted on all
129 participants at the Day Clinic for Cognitive Neurology of the University
130 Clinic Leipzig and the Max Planck Institute for Human and Cognitive and
131 Brain Sciences in order to include only healthy patients. The study
132 protocol was approved by the ethics committee of the University of
133 Leipzig (reference
134 154/13-ff). Data were obtained in accordance with the Declaration of
135 Helsinki.

136 **2.2 Recordings**

137 Resting state EEGs were recorded using 61 scalp electrodes (ActiCAP,
138 Brain Products GmbH, Gilching, Germany), and one additional VEOG
139 electrode for recording right eye activity. All electrodes were placed
140 according to the international standard 10–20 extended localization
141 system with FCz reference, digitized with a sampling frequency of $f_s=2500$
142 Hz, an amplitude resolution of 0.1 microV, and bandpass filtered between
143 0.015 Hz and 1 kHz. The ground was located at the sternum and scalp
144 electrode impedance was kept below 5 K Ω . Recordings took place in an
145 electrically shielded and sound-attenuated EEG booth. Here, 60s blocks
146 alternated between eyes open (EO) and eyes closed (EC) conditions for a
147 total recording of 16 min (8 blocks EC, 8 blocks EO, starting with EC).
148 During the EO condition, participants were asked to stay awake while
149 fixating their eyes on a black cross presented on a white background.

150 **2.3 Preprocessing**

151 The preprocessing steps are extensively described in [16], which we
152 summarize below. All EEG recordings were down-sampled from 2500 to
153 250 Hz and filtered between 1 and 45 Hz (8th order, Butterworth filter).
154 Blocks sharing the same condition were concatenated leading to the
155 creation of 2 datasets per subject. After visual inspection, outlying
156 channels were rejected and EEG segments presenting noise and/or
157 artefacts were removed (except eye movements and eye blinks that were
158 kept for further preprocessing). PCA was used to reduce data
159 dimensionality, by keeping PCs ($N \geq 30$) that explain 95% of the total data
160 variance. Then, independent component analysis (ICA) was performed

161 using the Infomax (runica) algorithm. Components reflecting eye
162 movement, eye blink or heartbeat related artefacts were removed.

163 Before performing microstate analysis, the following additional
164 preprocessing steps were conducted using MNE-python [18]: missing/bad
165 channels were interpolated using spherical spline interpolation, the
166 reference was re-projected to average and recordings were down-
167 sampled to 100Hz. Finally, each recording was filtered into broadband
168 plus the 5 traditional EEG frequency bands: broadband (1-30 Hz), delta (1-
169 4 Hz), theta (4-8 Hz), alpha (8-12 Hz), beta (15-30 Hz). Filter design
170 consisted of a two-pass forward and reverse, zero-phase, non-causal band-
171 pass FIR filter with the following parameters.

172 **Broadband:** - Lower passband edge: 1.00 - Lower transition
173 bandwidth: 1.00 Hz (-12 dB cutoff frequency: 0.50 Hz) - Upper passband
174 edge: 30.00 Hz
175 - Upper transition bandwidth: 7.50 Hz (-12 dB cutoff frequency: 33.75 Hz)
176 Filter length: 331 samples (3.310 sec)

177 **Delta:** - Lower passband edge: 1.00 - Lower transition bandwidth: 1.00
178 Hz (-12 dB cutoff frequency: 0.50 Hz) - Upper passband edge: 4.00 Hz -
179 Upper transition bandwidth: 2.00 Hz (-12 dB cutoff frequency: 5.00 Hz) -
180 Filter length: 331 samples (3.310 sec)

181 **Theta:** - Lower passband edge: 4.00 - Lower transition bandwidth: 2.00
182 Hz (-12 dB cutoff frequency: 3.00 Hz) - Upper passband edge: 8.00 Hz -
183 Upper transition bandwidth: 2.00 Hz (-12 dB cutoff frequency: 9.00 Hz) -
184 Filter length: 165 samples (1.650 sec)

185 **Alpha:** - Lower passband edge: 8.00 - Lower transition bandwidth: 2.00
186 Hz (-12 dB cutoff frequency: 7.00 Hz) - Upper passband edge: 12.00 Hz -
187 Upper transition bandwidth: 3.00 Hz (-12 dB cutoff frequency: 13.50 Hz) -
188 Filter length: 165 samples (1.650 sec)

189 **Beta:** - Lower passband edge: 15.00 - Lower transition bandwidth: 3.75
 190 Hz (-12 dB cutoff frequency: 13.12 Hz) - Upper passband edge: 30.00 Hz -
 191 Upper transition bandwidth: 7.50 Hz (-12 dB cutoff frequency: 33.75 Hz) -
 192 Filter length: 89 samples (0.890 sec)
 193 For all filters, a Hamming window with 0.0194 passband ripple and 53
 194 dB stopband attenuation was used to reduce border effects.

195 **2.4 MS segmentation**

196 **2.4.1 Segmentation**

197 Microstate segmentation was applied to each combination of frequency
 198 band (broadband, delta, theta, alpha, beta) x behavioural condition (EO,
 199 EC) leading to the computation of 10 optimal clusters using the
 200 methodology described below. First, local maxima of the Global Field
 201 Power (GFP) known to represent portions of EEG data with highest signal
 202 to noise ratio [19], were extracted from each individual recording. Then,
 203 20 epochs of 500 time points randomly drawn from the previous
 204 extraction were submitted to a modified k-means cluster analysis using
 205 the free academic software Cartool [20]. For each number of cluster
 206 centers K ranging from 1 to 12, 50 k-means initialisations were applied to
 207 each epoch. The initialisation with highest global explained variance
 208 (GEV) was selected and kept for further processing. A meta-criterion [21]
 209 was used to choose the optimal number of cluster centers k for each epoch.
 210 Individual optimal clusters were then merged within conditions and
 211 within frequencies to form 10 groups of 4060 clusters. Each group was
 212 then randomly re-sampled into 100 epochs of 5000 time points, and
 213 submitted to the same clustering algorithm (50 initialisations, with meta
 214 criterion selection), leading to the extraction of 100 optimal clusters per
 215 group. Finally, these 100 clusters were submitted to the modified K means

216 clustering algorithm to extract, for each number of cluster centroids k , a
217 set of maps which best represent the spatiotemporal variance of
218 frequency specific EEG data within each condition.

219 Selection of “common” MS maps

220 Given that we found high spatial correlations between MS maps across all
221 frequencies and EO/EC conditions, we fitted the broadband maps directly
222 to all the frequency bands in order to have a common reference. This may
223 be considered a heuristic approach for the sake of simplicity. An
224 alternative approach we explored was to perform subject-level (i.e. 1st
225 level) clustering on all data concatenated *within-subject* (across
226 frequencies, and/or conditions), followed by group-level (i.e. 2nd-level)
227 clustering. We found this to once again produce identical maps to the
228 broadband decomposition. This method could theoretically be used to find
229 the most “common” clusters across different datasets, in case of variable
230 k-means outputs (e.g. visually similar MS maps at different k -values). Since
231 it is beyond the scope of this paper, we leave it to future studies to validate
232 this method more rigorously.

233 **2.4.2 Fitting**

234 The common topographic maps selected above were then assigned to
235 every time point from all individual recordings using the traditional MS
236 back-fitting method [22]. First, the spatial correlation was computed
237 between every timepoint and map. Using the so called ‘winner takes all’
238 algorithm, each timepoint was labelled according to the map with which it
239 shared the highest absolute spatial correlation. Timepoints were labelled
240 as “non-assigned” when the absolute spatial correlation was below $r < 0.5$
241 threshold. To ensure temporal continuity of MS segmentation, a

smoothing step [17], [20] was applied. Finally, segments with duration shorter than 3 samples (30ms) were assigned to neighbouring segments using the following rule: the segment was split into two parts, where each part was assigned to the neighbouring segment with the higher spatial correlation. With backfitting completed, we extracted 4 spatiotemporal parameters for each microstate map, namely:

Global explained variance (Gev) described as the sum of variances of the original recording explained by the considered microstate map weighted by the Global Field Power at each moment in time. Units are percentages (%) between 0 and 1.

Mean spatial correlation (MeanSpatCorr) defined as the mean spatial correlation value between the assigned MS map and actual scalp topography at each timepoint. This results in a correlation coefficient $0 \leq r \leq 1$.

Mean duration (MeanDurs), defined as the mean temporal duration of segments assigned to each MS map. Units are in seconds (s).

Time coverage (TimeCov) is the ratio of time frames assigned to each MS map relative to the total number of time frames from the recording. Results are Units are percentages (%) between 0 and 1.

2.5 Adjusted Mutual information score

Scikit-learn [23] implementation of the adjusted mutual information score (AMI) [24] was used to quantify the mutual information (MI) shared between different MS temporal segmentations, whilst simultaneously accounting for random overlap due to chance. This metric, bounded between 0 and 1, is used to evaluate the statistical (in)dependence of two variables. In our case, AMI is estimated between the symbolic sequences of two different microstate segmentations (e.g. ABDCADB vs ABDBDAC).

269 A high score (approaching 1) indicates that the two segmentations agree
 270 on the temporal order of all labels while a low score (approaching 0)
 271 indicates that the segmentations' labels are not temporally aligned. We
 272 selected the corrected version of this metric in order to control for the
 273 impact of differences in label distribution due to chance (for example
 274 differences in overall time coverage between labels).

275

276 **2.6 Statistics**

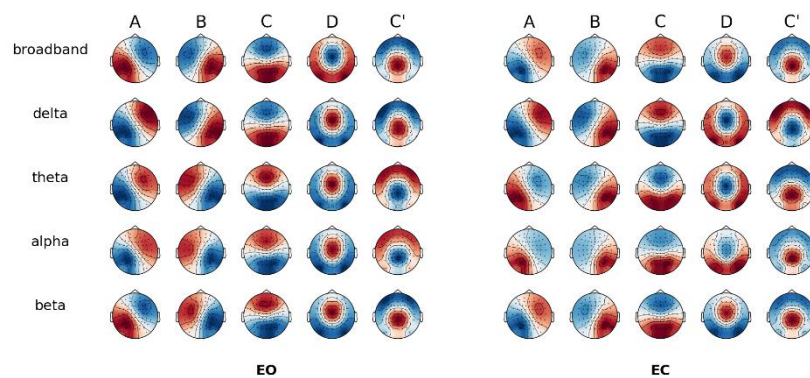
277 Statistical analyses were performed on the 4 main spatiotemporal
 278 parameters (Global explained variance, Mean spatial correlation, Mean
 279 duration, Time coverage). Tests were conducted using a two sided
 280 permutation test for equality of means on paired samples (same subject,
 281 either between condition, either between frequencies) under the H0
 282 hypothesis that both frequency (i.e. condition) share the same mean
 283 against the alternative H1 that the distributions come from two different
 284 populations. P-values were estimated by simulated random sampling with
 285 10000 replications. As a large number of statistical tests were carried out
 286 without specific pre-planned hypotheses [25], P values were corrected for
 287 multiple comparisons using the Bonferroni method. Corrected P-values
 288 are reported in the Results section, as well as the observed means (m) of
 289 both samples together with observed standard deviations. Effect sizes are
 290 reported as the standardised difference of means using Cohen's d (d).

291

292 3 Results

293 3.1 Spatial Similarity Analysis of Microstate Maps

294



295

296 Figure 1: MS segmentation parameters of MS topographies.

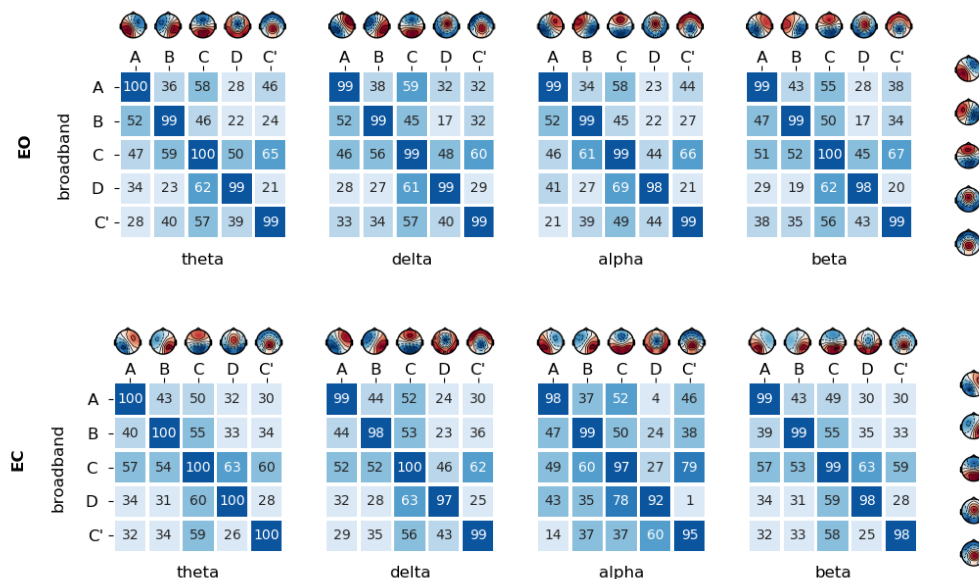
297 Global cluster centroids of each frequency band within each condition. Note
298 that polarity inversion is ignored in the classical analysis of spontaneous EEG.

299

300 Figure 1 illustrates the topographic results of MS segmentations in the
301 different conditions and frequency bands. After visual inspection of
302 optimal clusters at different cluster numbers (k), we identified that a value
303 of k=5 revealed five MS topographies that were similar across all EEG
304 bands and behavioural conditions, consistent with recent findings from
305 our laboratory [21], [26], [27]. MS maps were designated in line with the
306 canonical prototypes from the literature and their respective symbols,
307 featuring a left-right orientation (A), a right-left orientation (B), an
308 anterior-posterior orientation (C), fronto-central maximum (D) and
309 occipito-central (C') maximum.

310 Given the additional frequency dimension, we labelled the MS maps
311 firstly according to the Greek letters traditionally used for narrow-band

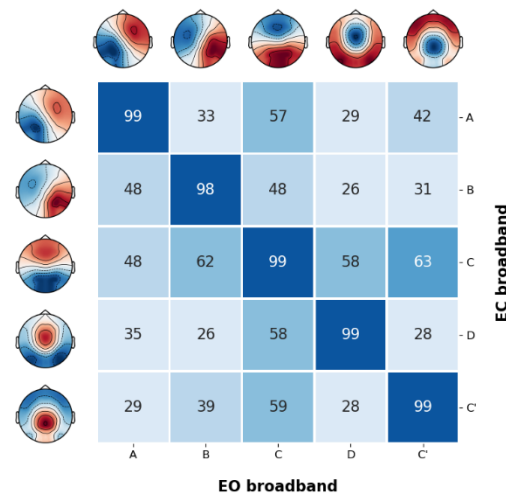
312 EEG (i.e. δ , θ , α , β) and then the Latin alphabet for the canonical map
 313 symbols (i.e. A, B, C, D). For example, αA denoted the left-right diagonal
 314 map from the alpha band (α) segmentation, and δC the anterior-posterior
 315 map from the delta band (δ) segmentation. The broadband segmentation
 316 was designated with the prefix 'bb'
 317



318
 319 Figure 2: MS segmentation parameters of MS topographies.
 320 Spatial correlation of cluster centers of each sub-frequency bands compared to
 321 broadband for eyes opened (EO) and eyes closed (EC) condition.

322
 323 As shown in Figure 2, when comparing topographies between
 324 broadband and each narrow-band (i.e. the diagonal entries in the
 325 correlation matrix), all spatial correlations were $r > 0.98$. Consequently,
 326 we fitted the broadband maps directly to all the frequency bands in order
 327 to have a common reference.

328
 329



330

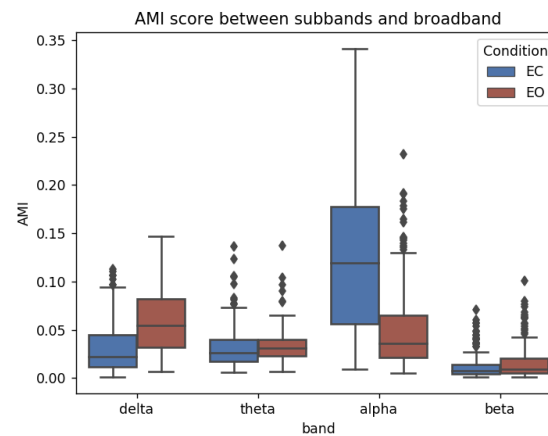
331 Figure 3: MS segmentation parameters of MS topographies.

332 Spatial correlation of broadband cluster centers between eyes opened (EO) and
333 eyes closed (EC) condition.

334

335 We similarly observed common MS maps when comparing broadband
336 topographies between EO and EC conditions (Figure 3), with all intraclass
337 spatial correlations exceeding $r > 0.98$, thus providing justification for
338 comparing microstate parameters between behavioural conditions while
339 fitting condition specific broadband maps.

3.2 Mutual information

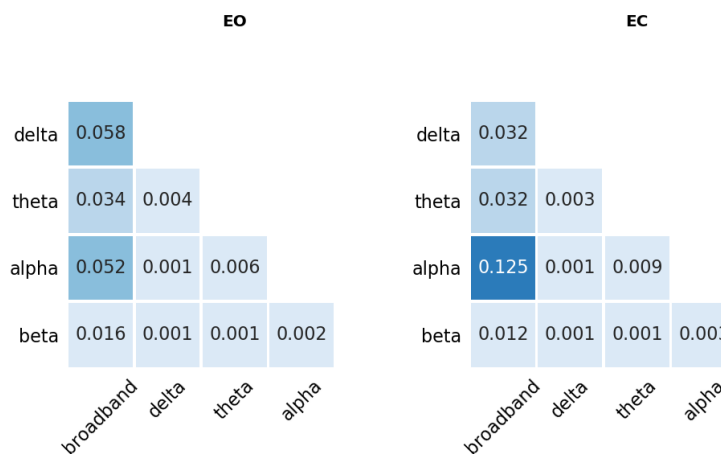


341

342 Figure 4: Adjusted mutual information between band segmentations.

343 Mean adjusted mutual information is depicted between broadband and narrow-

344 band segmentations, for each behavioural condition. n = 203 subjects.



345 Figure 5: Mean adjusted mutual information between band
346 segmentations.

347 Mean (n = 203 subjects) adjusted mutual information for all frequency pairs.

348

349 Concisely, Adjusted Mutual Information (AMI, bounded between 0 and
350 1) is an index of how similar two separate MS segmentations are, by
351 estimating the degree of shared information (i.e. the number of time
352 points assigned with the same MS) between their symbolic sequences (e.g.
353 ABCD vs ABDA). The 'adjusted' aspect ensures the measure is unbiased for
354 symbolic overlap(s) due to chance when cluster numbers are low (as is the
355 case here given $k=5$) [24]. Higher AMI (approaching 1) indicates nearly
356 identical MS temporal sequences, while lower AMI (approaching 0)
357 indicates temporally independent sequences. (i.e. low overlap)

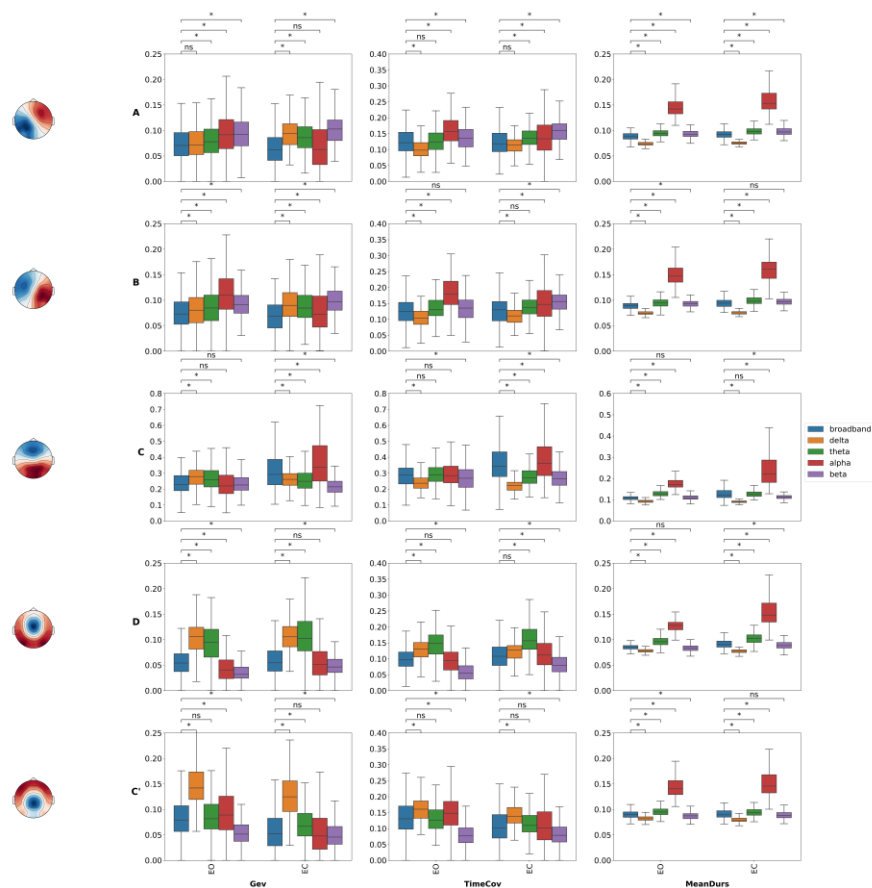
358 As shown in Figures 4 and 5, the AMI between broadband and narrow-
359 band segmentations in the EO condition showed a value of $s = 0.06$ for
360 delta, $s = 0.03$ for theta, $s = 0.05$ for alpha, and $s = 0.01$ for beta. These
361 values are surprisingly low and we can conclude that the broadband
362 segmentation is comparatively independent of the narrow EEG bands. A
363 similar conclusion can be made by examining the AMI between the
364 narrow-bands *themselves*, with a maximum AMI value between theta and
365 alpha bands (EO: $s = 0.006$, EC: $s = 0.009$), and a minimum AMI value of s
366 = 0.001 for non-adjacent EEG bands (delta-alpha, delta-beta, theta-beta)

367 As a sanity check, inspecting the EO vs EC transition, shared
368 information with broadband decreased for the delta band ($s = 0.03$) but
369 increased for the alpha band ($s = 0.12$). The latter is in line with
370 predictions, as alpha oscillations are known to increase considerably
371 during eye closure, which would amplify their contribution to the
372 broadband signal and consequently their shared dynamics.

373

374 3.3 Across Frequency comparison

375



376

377 Figure 6: MS segmentation parameters of MS topographies.

378 Mean global explained variance (Gev), microstate time coverage (time coverage)
 379 and mean segment duration (MeanDurs, in s) within each microstate
 380 configuration (A – C') for each frequency band (broadband, delta, theta, alpha,
 381 beta) for both eyes closed condition and eyes opened condition. Significance

values are indicated from paired permutation test on mean between conditions.
ns: $0.05 < p$, * $0.01 < p \leq 0.05$.

Boxplots consist of median (Q2), first quartile (Q1), third quartile (Q3), maximum ($Q3 + 1.5 \cdot (Q3 - Q1)$), minimum ($Q1 - 1.5 \cdot (Q3 - Q1)$). Scales of Microstates C metrics are different from others states due to difference of order of magnitude.

All subsequent results were computed using paired permutation tests and Bonferroni correction for $c = 120$ comparisons. In addition to Fig 6, p -values and effect sizes are reported in Table 1 of the Supplementary Results.

In summary, only 23 of the 120 pairwise comparisons between broadband and narrow-band MS measures (Global explained variance (Gev), Mean spatial correlation, Mean duration (MeanDurs), Time coverage (TimeCov) *did not* meet the threshold for a statistical significant effect. As can be seen from Fig 6, these include Gev for δA , αC , βC , $\theta C'$, in EO and αA , αD , $\alpha C'$, in EC.

TimeCov for θA , βB , θC , αC , αD , $\theta C'$, in EO and δA , θB , δD , $\theta C'$, $\alpha C'$, in EC.

MeanDurs for βC , βD , in EO and βB , θC , $\beta C'$, in EC.

The majority of pairwise comparisons with broadband (97) were found to be statistically significant, some of them with large effect sizes, in particular:

In the EC condition, mean duration of map A was longer ($d = 3.38$, $p < 0.05$) in alpha (αA , 150 ms) compared to broadband (bbA, 90 ms). On the other hand, mean duration of map B was shorter ($d = -2.08$, $p < 0.05$) in delta (δB , 80 ms) compared to broadband (bbB, 90 ms), while map C duration was longer ($d = 1.33$, $p < 0.05$) in theta (θC , 130 ms) compared to

411 broadband (bbC, 110 ms). Relative time coverage of map D was lower (d
412 = -1.14, $p < .05$) in beta (βD , 6 %) compared to broadband (bbD, 10%).
413
414 In the EO condition, mean duration of map B was shorter (d = -1.69, $p <$
415 0.05) in delta (δB , 74 ms) compared to broadband (bbB, 89 ms), but was
416 longer (d = 3.25, $p < 0.05$) in alpha (αB , 151ms). In terms of time coverage,
417 map D had a lower (d = -1.14, $p < 0.05$) presence in the beta band (βD , 5%)
418 compared to broadband (bbD, 10%) while its presence was increased (d =
419 1.02, $p < 0.05$) in theta frequencies. (θD 15%) *Microstate C'* demonstrated
420 more explained variance (d = -1.44, $p < 0.05$) in the delta band ($\delta C'$, 11%)
421 compared to broadband (bbC' , 6%)
422

3.4 Within Frequency comparison

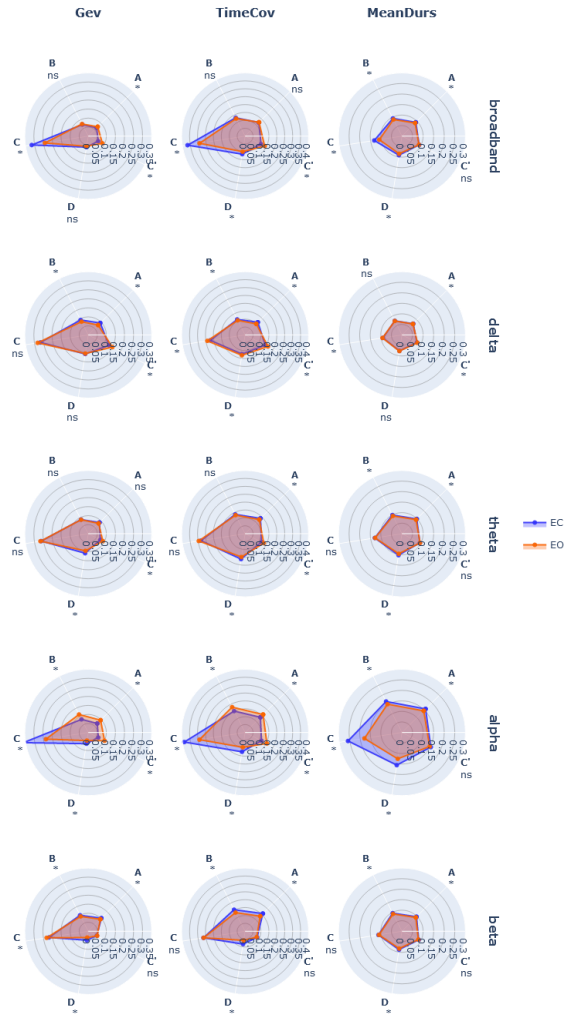


Figure 7: MS segmentation parameters of different frequency bands.

Mean global explained variance (Gev), microstate time coverage (time coverage) and mean segment duration (MeanDurs, in s) for each microstate (A – C') within each frequency band (broadband, delta, theta, alpha, beta) for both

431 eyes closed condition (EC, blue) and eyes opened condition (EO, red).
432 Significance values are indicated from paired permutation test on mean between
433 conditions.

434 $ns : 0.05 < p, * \text{ for } 0.01 < p \leq 0.05$

435

436 In this section, we directly compared EO vs EC condition within each
437 frequency band, and only relevant cases where narrow-band measures
438 were distinctly different compared to the broadband analysis are reported
439 (Figure 7). The full results are documented in Table 2 of the
440 Supplementary Results.

441 For time coverage (TimeCov), map A was relatively more prevalent in
442 EO vs EC in the alpha band ($d = 0.57, p < .05$) than for broadband ($d = 0.24,$
443 $p < .05$). Conversely, map C coverage was less prevalent in alpha ($sd = -$
444 $1.00, p < .05$) than broadband ($d = -0.71, p < .05$)

445 Some narrow-band effects were found to be opposite compared to
446 broadband : βA TimeCov had decreased prevalence ($d = -0.48, p < .05$) in
447 EO vs EC , while bbA TimeCov showed an increase ($d = 0.24, p < .05$). βC
448 TimeCov had increased prevalence ($d = 0.21, p < 0.05$) in EO vs EC, while
449 bbC TimeCov showed a decrease ($d = -0.71, p < .05$).

450 Finally significant EO vs EC effects were found in the narrow-band
451 analyses which were not evident in the broadband case: a decrease ($d = -$
452 $0.31, p < 0.05$) in *Gev of map B was observed in the beta band* while no
453 significant effect was found for broadband. Likewise in beta, map A
454 TimeCov was decreased ($d = -0.51, p < 0.05$) in EO vs EC, while broadband
455 TimeCov was non-significant ($p = 1.0, n.s.$).

456

457 **4 Discussion**

458
 459 Historically, the first microstate (MS) analysis was applied by Lehmann
 460 and colleagues to narrowband (alpha) oscillations [2], yet this “frequency-
 461 specific” approach appears to have been overlooked during the last
 462 decades of MS research in favour of decomposing broadband (e.g. 2-40
 463 Hz) EEG signals. Hence, the present study specifically explored the MS
 464 characteristics of narrow-band EEG signals, their quantitative
 465 interrelationship, and whether they provide any novel information
 466 compared to course-grained broadband dynamics. This was done by first
 467 filtering the broadband EEG signal into several narrow-band frequencies
 468 (delta, theta, alpha, and beta), with the goal of comparing MS symbolic
 469 sequences and classical measures (explained variance, mean duration,
 470 time coverage) between them, as well as across different behavioural
 471 conditions (eyes open (EO) vs eyes closed (EC)).

472 473 **4.1 Topographic patterns**

474 We first investigated whether analogous MS scalp topographies would be
 475 produced by segmenting broadband versus narrow-band EEG signals
 476 (including the alpha band [28]). Interestingly, we observed highly similar
 477 MS topographies (with minimum spatial correlations of $r > 0.98$) across all
 478 investigated broad- and narrow- band frequencies (broadband, delta to
 479 beta), as well as between EO/EC conditions. This is compatible with recent
 480 work by Brechet and colleagues [27], who observed that states of sleep
 481 and wake exhibited significantly different spectral content (e.g. delta vs
 482 beta power) but very similar MS maps. Moreover, these maps
 483 corresponded to the canonical (broadband) topographies previously
 484 described in the literature [1], [29]. It is therefore tempting to assume that

identical neuronal sources are involved in generating the same topographies across frequencies. However, although different maps imply different generators (forward problem), same topographies do not necessarily imply identical generators (inverse problem). Due to the ill-posed nature of EEG signals (constructive and destructive electromagnetic fields), similar scalp potentials can still be generated by different underlying brain mechanisms [30]. Hence, although we cannot unequivocally conclude that MS maps across the EEG spectrum are generated by the same brain sources operate, this would be the most probable and parsimonious interpretation. Moreover, we must juxtapose our findings with work from other groups [6] which applied a similar approach but didn't necessarily find the same topographies across the EEG spectrum. From a methodological point of view, it should be kept in mind that narrow-band MS analysis does not *per se* require similar topographies between frequencies. In this case, although cross frequency comparisons would not be possible due to dissimilar maps, it would remain valid to study and quantify spatiotemporal MS parameters within each frequency band separately, for example, in the service of clinical biomarker discovery [4]. Reassuringly, the MS maps of our study replicate the ones derived from independent work utilising the same EEG dataset [3], further supporting the reproducibility of MS analysis despite methodological variations between studies (e.g. absence of resampling).

4.2 Mutual information

Milz and colleagues [28] recently proposed that alpha oscillations were the major component driving microstate dynamics. In general, adjusted mutual information (AMI) analyses reported in our work reveal low values (near or below 0.1) of information shared between the narrow-band segmentations, including alpha, and that of the broadband

decomposition. However, consistent with the work of Milz and colleagues [28], the alpha-band during eyes-closed (EC) did indeed have the highest shared information with broadband (around 0.125). Importantly however, this relationship did not necessarily hold during eyes-open (delta being highest). This indicates specific narrow-band contribution(s) to broadband dynamics heavily depend on behavioural state. Moreover, if narrow-band(s) topographies were directly responsible for the origin of the spatial distribution of the broadband signal, one would expect much higher AMI values (at least 0.5) than those, we observed. In view of the results presented, it would be inaccurate to claim that alpha band, or any other narrow-band as the dominant source of broadband topographies.

In contrast, our results appear to support the ideas of Croce and colleagues [31], who suggested that broadband MS dynamics could not be extrapolated from one or a subset of EEG frequency bands. It remains unclear how the interaction of several narrow-band-components leads to a substantially different broadband MS decomposition. We speculate that this might stem from the fact that i) different narrow band signals could cancel each other at specific time points and ii) microstate assignment is non-linear given the winner-takes all approach.

Lastly and most intriguingly, no significant informational interrelations were found between the narrow-band topographical dynamics themselves (e.g. delta vs beta, theta vs alpha), indicating that each EEG band appears to have its own independent dynamics. This may not be surprising, considering that spontaneous EEG oscillations have been reported to dynamically switch from a resting signatures (e.g. alpha) to task-specific active mode(s) dominated by theta [11], beta [32] or gamma activities [12]). In this context, our observations of spatiotemporal independence between narrow-band EEG components support the operation of “oscillatory multiplexing” [13] mechanisms in the cortex,

542 whereby brain regions could combine different frequencies for
543 integrating/segregating information across large-scale networks [33]
544

545 **4.3 Classical microstate parameters**

546 Microstates are defined as short periods of time during which the scalp
547 electric field remains quasi-stable. Traditional microstate analysis does
548 not suggest specific frequency filtering, thus resulting in various filters
549 settings across studies [1]. Our findings show that quasi stable structures
550 (around 80ms or longer) are present in all studied bands. It is established
551 that such spatiotemporal structures do not appear for randomly shuffled
552 EEG [34]. For most EEG narrow-bands, mean MS durations were usually
553 in the same range as the typically reported 70–120 ms, but often longer
554 (for example, alpha in EC was about 150 ms). It is therefore interesting to
555 consider the mechanistic links between the course-grained broadband
556 dynamics of the brain's microstates and the dynamics of different
557 frequency-specific modes.

558 **4.4 Between condition comparison: toward a** 559 **systematic frequency decomposition of microstate** 560 **dynamics?**

561 A total of about one third (22 of 75) of pairwise comparisons between
562 eyes open and eyes closed conditions revealed significant effects. Within
563 each frequency, between 14 (for alpha) and 8 (for theta) of the studied
564 parameters were found significant. Compared to the narrow-band results,
565 the classical broadband MS parameters had a higher effect size for only
566 one parameter (broadband microstate B mean duration). For all other 14

parameters, at least one narrow-band component showed a relatively stronger effect size.

The addition of the frequency dimension therefore has the primary benefit of increasing the number of potential markers that could aid clinical prognosis or for the understanding of brain mechanisms. Hence, the extra frequency dimension could in itself lead to more fine-grained explorations of the multiplex EEG signal than the more general broadband analysis. It remains for future work to investigate the statistical power and effect sizes of these markers compared to those studied traditionally.

Moreover, narrow-band effects were sometimes found to be opposite to the broadband analysis, hence limiting the analysis to the latter could lead to incorrect or incomplete interpretations of underlying brain dynamics. We expect that future studies will explore the neurophysiological significance of narrowband MS analysis more deeply.

4.5 Potential Limitations and Future Work

We consider to current findings exploratory, considering the large number of tests that were carried out and in the absence of well-defined hypotheses. Nevertheless, we carried out Bonferroni correction, which may be considered the most conservative method for controlling multiple comparisons. Several studies have thus far proposed explanations for the origins of broadband MS topographies [7]. We feel it is still too early to make analogies or speculations between these results and those of the narrow-band dynamics. However, we believe that the application of the methodology proposed here may lead to valuable insights in order to more fully understand the underlying spectral tapestry of EEG microstates.

593 **5 Conclusion**

594 Ultimately, we report a number of important new findings between the
595 classical broadband MS analysis, usually performed in the EEG field, and
596 its application to more narrow frequency bands relevant to cortical
597 oscillatory activities. In a nutshell, it appears that each canonical EEG
598 frequency band possesses its own spatiotemporal dynamics, and that
599 broadband dynamics cannot be appropriately explained by individual
600 narrow-band frequency components.

601 Analysis of narrow-band MS parameters revealed spatial and temporal
602 characteristics that both converged and diverged from broadband MS
603 findings. At the very least, our results indicate that narrow-band analysis
604 is justified as complementary to the usual broadband MS analysis. A
605 narrow-band decomposition into frequencies more specific for cortical
606 oscillatory activity could not only advance and/or consolidate findings in
607 clinical disorders e.g. [4] [6], but also enable a better understanding of the
608 organization and functioning of large-scale brain dynamics.

609 **Credit authorship contribution statement**

610 **Victor Férat:** Conceptualization, Formal analysis, Methodology,

611 Visualization, Writing - original draft, Writing - review & editing.

612 **Martin Seeber:** Writing - review & editing

613 **Christoph Michel:** Writing - review & editing

614 **Tomas Ros:** Writing - Conceptualization, Formal analysis, Methodology
615 review & editing.

616 **Acknowledgments**

We would like to thank the Mind-Body-Emotion group at the Max Planck Institute for Human Cognitive and Brain Sciences for all the work they have done to make their dataset public. The study was supported by the Swiss National Science Foundation (NCCR Synapsy grant No. 51NF40 – 185897 and grant No. 320030_184677) to CMM.

Conflict of Interest Statement

The authors declare that the research was conducted in the absence of any commercial or financial relationships that could be construed as a potential conflict of interest.

References

- [1] C. M. Michel and T. Koenig, 'EEG microstates as a tool for studying the temporal dynamics of whole-brain neuronal networks: A review', *NeuroImage*, vol. 180, pp. 577–593, Oct. 2018, doi: 10.1016/j.neuroimage.2017.11.062.
- [2] D. Lehmann, 'Multichannel topography of human alpha EEG fields', *Electroencephalogr. Clin. Neurophysiol.*, vol. 31, no. 5, pp. 439–449, 1971.
- [3] A. P. Zanesco, B. G. King, A. C. Skwara, and C. D. Saron, 'Within and between-person correlates of the temporal dynamics of resting EEG microstates', *NeuroImage*, vol. 211, p. 116631, May 2020, doi: 10.1016/j.neuroimage.2020.116631.
- [4] E. L. Merrin, P. Meek, T. C. Floyd, and E. Callaway III, 'Topographic segmentation of waking EEG in medication-free schizophrenic patients', *Int. J. Psychophysiol.*, vol. 9, no. 3, pp. 231–236, 1990.
- [5] E. Javed, P. Croce, F. Zappasodi, and C. Del Gratta, 'Hilbert spectral analysis of EEG data reveals spectral dynamics associated with microstates', *J. Neurosci. Methods*, vol. 325, p. 108317, 2019.
- [6] C. S. Musaeus *et al.*, 'Changes in the left temporal microstate are a sign of cognitive decline in patients with Alzheimer's disease', *Brain Behav.*, p. e01630, 2020.
- [7] J. Britz, D. Van De Ville, and C. M. Michel, 'BOLD correlates of EEG topography reveal rapid resting-state network dynamics',

- 653 *NeuroImage*, vol. 52, no. 4, pp. 1162–1170, Oct. 2010, doi:
654 10.1016/j.neuroimage.2010.02.052.
- 655 [8] D. M. Groppe *et al.*, ‘Dominant frequencies of resting human brain
656 activity as measured by the electrocorticogram’, *NeuroImage*, vol. 79,
657 pp. 223–233, Oct. 2013, doi: 10.1016/j.neuroimage.2013.04.044.
- 658 [9] M. S. Mellem, S. Wohltjen, S. J. Gotts, A. S. Ghuman, and A. Martin,
659 ‘Intrinsic frequency biases and profiles across human cortex’, *J.*
660 *Neurophysiol.*, vol. 118, no. 5, pp. 2853–2864, 2017.
- 661 [10] A. Keitel and J. Gross, ‘Individual human brain areas can be identified
662 from their characteristic spectral activation fingerprints’, *PLoS Biol.*,
663 vol. 14, no. 6, p. e1002498, 2016.
- 664 [11] U. Ribary, S. M. Doesburg, and L. M. Ward, ‘Unified principles of
665 thalamo-cortical processing: the neural switch’, *Biomed. Eng. Lett.*,
666 vol. 7, no. 3, pp. 229–235, Aug. 2017, doi: 10.1007/s13534-017-
667 0033-4.
- 668 [12] J. F. Hipp, A. K. Engel, and M. Siegel, ‘Oscillatory Synchronization in
669 Large-Scale Cortical Networks Predicts Perception’, *Neuron*, vol. 69,
670 no. 2, pp. 387–396, Jan. 2011, doi: 10.1016/j.neuron.2010.12.027.
- 671 [13] T. Akam and D. M. Kullmann, ‘Oscillatory multiplexing of population
672 codes for selective communication in the mammalian brain’, *Nat.*
673 *Rev. Neurosci.*, vol. 15, no. 2, pp. 111–122, Feb. 2014, doi:
674 10.1038/nrn3668.
- 675 [14] J. J. Schulman, R. Cancro, S. Lowe, F. Lu, K. D. Walton, and R. R. Llinás,
676 ‘Imaging of Thalamocortical Dysrhythmia in Neuropsychiatry’,
677 *Front. Hum. Neurosci.*, vol. 5, 2011, doi: 10.3389/fnhum.2011.00069.
- 678 [15] T. Ros *et al.*, ‘Neurofeedback Tunes Scale-Free Dynamics in
679 Spontaneous Brain Activity’, *Cereb. Cortex*, p. cercor;bhw285v1, Sep.
680 2016, doi: 10.1093/cercor/bhw285.
- 681 [16] A. Babayan *et al.*, ‘A mind-brain-body dataset of MRI, EEG, cognition,
682 emotion, and peripheral physiology in young and old adults’, *Sci.*
683 *Data*, vol. 6, p. 180308, 2019.
- 684 [17] R. D. Pascual-Marqui, C. M. Michel, and D. Lehmann, ‘Segmentation of
685 brain electrical activity into microstates: model estimation and
686 validation’, *IEEE Trans. Biomed. Eng.*, vol. 42, no. 7, pp. 658–665,
687 1995.
- 688 [18] A. Gramfort *et al.*, ‘MEG and EEG data analysis with MNE-Python’,
689 *Front. Neurosci.*, vol. 7, p. 267, 2013.
- 690 [19] T. Koenig and D. Brandeis, ‘Inappropriate assumptions about EEG
691 state changes and their impact on the quantification of EEG state
692 dynamics’, *Neuroimage*, vol. 125, pp. 1104–1106, 2016.
- 693 [20] D. Brunet, M. M. Murray, and C. M. Michel, ‘Spatiotemporal analysis
694 of multichannel EEG: CARTOOL’, *Comput. Intell. Neurosci.*, vol. 2011,
695 2011.

- 696 [21] L. Bréchet, D. Brunet, G. Birot, R. Gruetter, C. M. Michel, and J. Jorge,
697 'Capturing the spatiotemporal dynamics of self-generated, task-
698 initiated thoughts with EEG and fMRI', *Neuroimage*, vol. 194, pp. 82–
699 92, 2019.
- 700 [22] D. Van De Ville, J. Britz, and C. M. Michel, 'EEG microstate sequences
701 in healthy humans at rest reveal scale-free dynamics', *Proc. Natl.*
702 *Acad. Sci.*, vol. 107, no. 42, pp. 18179–18184, Oct. 2010, doi:
703 10.1073/pnas.1007841107.
- 704 [23] F. Pedregosa *et al.*, 'Scikit-learn: Machine Learning in Python', *J.*
705 *Mach. Learn. Res.*, vol. 12, pp. 2825–2830, 2011.
- 706 [24] N. X. Vinh, J. Epps, and J. Bailey, 'Information theoretic measures for
707 clusterings comparison: Variants, properties, normalization and
708 correction for chance', *J. Mach. Learn. Res.*, vol. 11, pp. 2837–2854,
709 2010.
- 710 [25] R. A. Armstrong, 'When to use the Bonferroni correction',
711 *Ophthalmic Physiol. Opt.*, vol. 34, no. 5, pp. 502–508, 2014.
- 712 [26] D. F. D'Croz-Baron, M. Baker, C. M. Michel, and T. Karp, 'EEG
713 Microstates Analysis in Young Adults With Autism Spectrum
714 Disorder During Resting-State', *Front. Hum. Neurosci.*, vol. 13, p. 173,
715 Jun. 2019, doi: 10.3389/fnhum.2019.00173.
- 716 [27] L. Bréchet, D. Brunet, L. Perogamvros, G. Tononi, and C. M. Michel,
717 'EEG microstates of dreams', *Sci. Rep.*, vol. 10, no. 1, p. 17069, Dec.
718 2020, doi: 10.1038/s41598-020-74075-z.
- 719 [28] P. Milz, R. D. Pascual-Marqui, P. Achermann, K. Kochi, and P. L. Faber,
720 'The EEG microstate topography is predominantly determined by
721 intracortical sources in the alpha band', *Neuroimage*, vol. 162, pp.
722 353–361, 2017.
- 723 [29] A. Custo, D. Van De Ville, W. M. Wells, M. I. Tomescu, D. Brunet, and C.
724 M. Michel, 'Electroencephalographic resting-state networks: source
725 localization of microstates', *Brain Connect.*, vol. 7, no. 10, pp. 671–
726 682, 2017.
- 727 [30] H. von Helmholtz, 'Ueber einige Gesetze der Vertheilung elektrischer
728 Strome in körperlichen Leitern, mit Anwendung auf die thierisch-
729 elektrischen Versuche (Schluss.)', *Ann. Phys.*, vol. 165, no. 7, pp. 353–
730 377, 1853.
- 731 [31] P. Croce, A. Quercia, S. Costa, and F. Zappasodi, 'EEG microstates
732 associated with intra-and inter-subject alpha variability', *Sci. Rep.*,
733 vol. 10, no. 1, pp. 1–11, 2020.
- 734 [32] T. Fernández *et al.*, 'EEG activation patterns during the performance
735 of tasks involving different components of mental calculation',
736 *Electroencephalogr. Clin. Neurophysiol.*, vol. 94, no. 3, pp. 175–182,
737 Mar. 1995, doi: 10.1016/0013-4694(94)00262-J.

- 738 [33] M. Le Van Quyen, 'The brainweb of cross-scale interactions', *New*
739 *Ideas Psychol.*, vol. 29, no. 2, pp. 57–63, Aug. 2011, doi:
740 10.1016/j.newideapsych.2010.11.001.
- 741 [34] J. Wackermann, D. Lehmann, C. Michel, and W. Strik, 'Adaptive
742 segmentation of spontaneous EEG map series into spatially defined
743 microstates', *Int. J. Psychophysiol.*, vol. 14, no. 3, pp. 269–283, 1993.
744
746

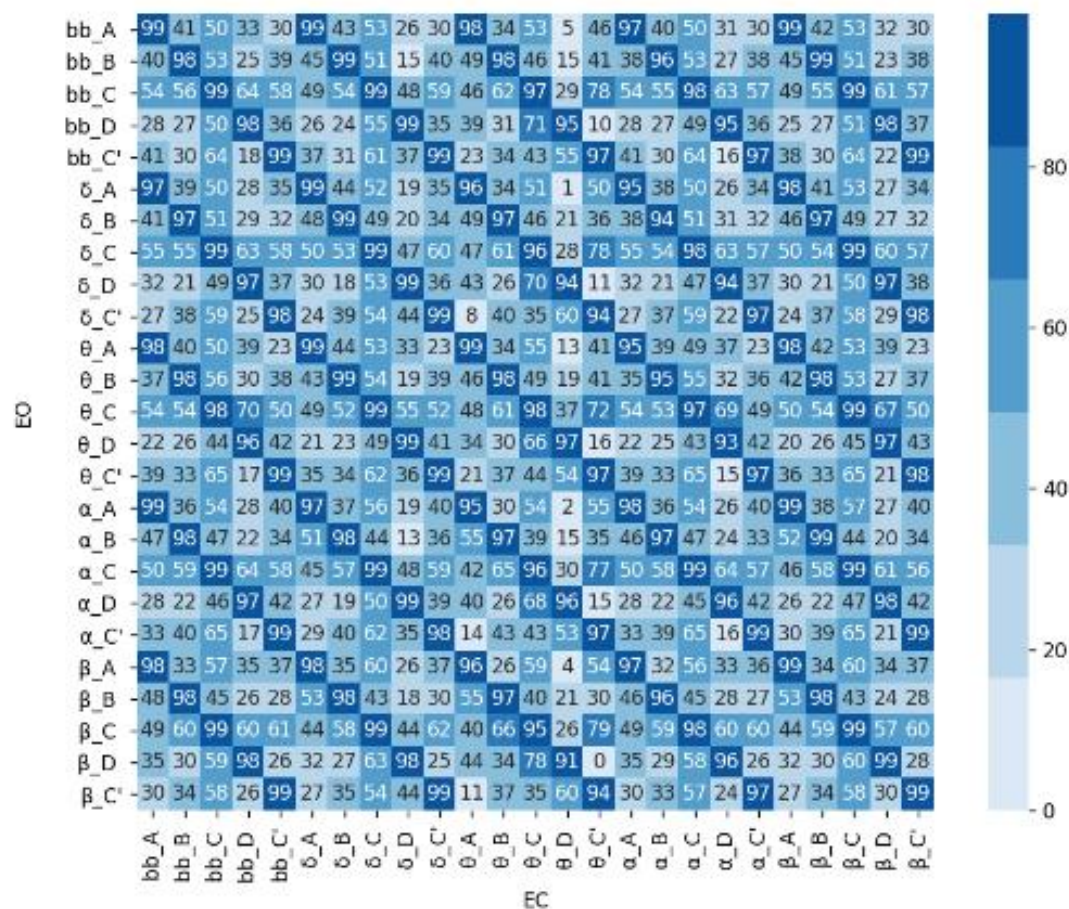


Figure : MS segmentation parameters of MS topographies.

Spatial correlation of cluster centers between eyes opened (EO) and eyes closed (EC) condition across all frequency bands.

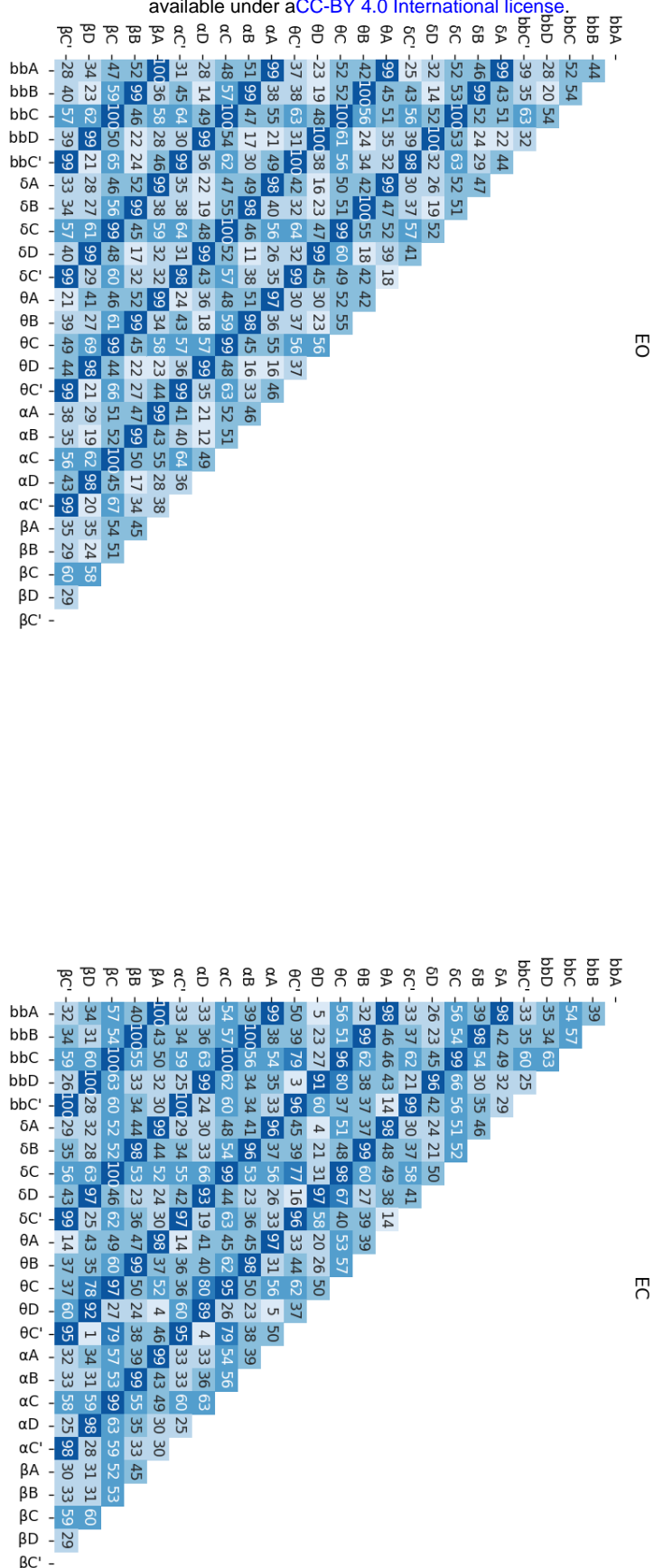


Figure: MS segmentation parameters of MS topographies.
Spatial correlation of cluster centers between all frequency bands in both EO and EC conditions.

EO

EC

map	band1	metric	d	p
A	alpha	Gev	0.57	0.02
		MeanDurs	3.38	0.02
		TimeCov	0.76	0.02
	beta	Gev	0.61	0.02
		MeanDurs	0.47	0.02
		TimeCov	0.23	0.02
	delta	Gev	0.11	1.00
		MeanDurs	-1.80	0.02
		TimeCov	-0.66	0.02
	theta	Gev	0.22	0.02
		MeanDurs	0.62	0.02
		TimeCov	0.05	1.00
B	alpha	Gev	0.94	0.02
		MeanDurs	3.25	0.02
		TimeCov	1.13	0.02
	beta	Gev	0.56	0.02
		MeanDurs	0.37	0.02
		TimeCov	0.18	0.17
	delta	Gev	0.20	0.05
		MeanDurs	-1.69	0.02
		TimeCov	-0.56	0.02
	theta	Gev	0.32	0.02
		MeanDurs	0.58	0.02
		TimeCov	0.17	0.05
C	alpha	Gev	-0.06	1.00
		MeanDurs	2.31	0.02
		TimeCov	0.00	1.00
	beta	Gev	-0.13	1.00
		MeanDurs	0.10	1.00
		TimeCov	-0.30	0.02
	delta	Gev	0.50	0.02
		MeanDurs	-1.28	0.02
		TimeCov	-0.71	0.02
	theta	Gev	0.31	0.02
		MeanDurs	1.33	0.02
		TimeCov	0.06	1.00
C'	alpha	Gev	0.25	0.02
		MeanDurs	2.41	0.02
		TimeCov	0.25	0.02
	beta	Gev	-0.87	0.02
		MeanDurs	-0.30	0.02
		TimeCov	-1.10	0.02
	delta	Gev	1.32	0.02
		MeanDurs	-0.91	0.02
		TimeCov	0.45	0.02
	theta	Gev	0.06	1.00
		MeanDurs	0.52	0.02
		TimeCov	-0.12	1.00
D	alpha	Gev	-0.40	0.02
		MeanDurs	3.23	0.02
		TimeCov	-0.11	1.00
	beta	Gev	-0.91	0.02
		MeanDurs	-0.17	0.60
		TimeCov	-1.14	0.02
	delta	Gev	1.44	0.02
		MeanDurs	-0.91	0.02
		TimeCov	0.81	0.02
	theta	Gev	1.06	0.02
		MeanDurs	1.06	0.02
		TimeCov	1.02	0.02

map	band1	metric	d	p
A	alpha	Gev	0.12	0.10
		MeanDurs	3.25	0.02
		TimeCov	0.28	0.02
	beta	Gev	1.12	0.02
		MeanDurs	0.44	0.02
		TimeCov	0.83	0.02
	delta	Gev	0.88	0.02
		MeanDurs	-2.00	0.02
		TimeCov	-0.24	0.14
	theta	Gev	0.66	0.02
		MeanDurs	0.55	0.02
		TimeCov	0.38	0.02
B	alpha	Gev	0.22	0.02
		MeanDurs	2.91	0.02
		TimeCov	0.38	0.02
	beta	Gev	0.82	0.02
		MeanDurs	0.19	0.14
		TimeCov	0.48	0.02
	delta	Gev	0.60	0.02
		MeanDurs	-2.08	0.02
		TimeCov	-0.49	0.02
	theta	Gev	0.46	0.02
		MeanDurs	0.43	0.02
		TimeCov	0.16	0.48
C	alpha	Gev	0.34	0.02
		MeanDurs	1.50	0.02
		TimeCov	0.16	0.02
	beta	Gev	-1.00	0.02
		MeanDurs	-0.76	0.02
		TimeCov	-1.00	0.02
	delta	Gev	-0.48	0.02
		MeanDurs	-1.64	0.02
		TimeCov	-1.53	0.02
	theta	Gev	-0.50	0.02
		MeanDurs	-0.08	1.00
		TimeCov	-0.83	0.02
C'	alpha	Gev	0.00	1.00
		MeanDurs	2.50	0.02
		TimeCov	0.05	1.00
	beta	Gev	-0.24	0.02
		MeanDurs	-0.20	0.24
		TimeCov	-0.54	0.02
	delta	Gev	1.52	0.02
		MeanDurs	-1.17	0.02
		TimeCov	0.63	0.02
	theta	Gev	0.31	0.02
		MeanDurs	0.31	0.02
		TimeCov	0.07	1.00
D	alpha	Gev	0.02	1.00
		MeanDurs	2.44	0.02
		TimeCov	0.14	0.02
	beta	Gev	-0.40	0.02
		MeanDurs	-0.30	0.02
		TimeCov	-0.73	0.02
	delta	Gev	1.26	0.02
		MeanDurs	-1.47	0.02
		TimeCov	0.17	1.00
	theta	Gev	1.15	0.02
		MeanDurs	0.81	0.02
		TimeCov	0.87	0.02

Table 1: For both EO and EC condition, P values (p) and cohen's d (d) are reported for each test between broadband and band segmentation on each studied metric (Global explained variance, Mean duration, time coverage).

map	band	metric	d	p
A	alpha	Gev	0.12	0.10
		MeanDurs	3.25	0.02
		TimeCov	0.28	0.02
	beta	Gev	1.12	0.02
		MeanDurs	0.44	0.02
		TimeCov	0.83	0.02
	delta	Gev	0.88	0.02
		MeanDurs	-2.00	0.02
		TimeCov	-0.24	0.14
	theta	Gev	0.66	0.02
		MeanDurs	0.55	0.02
		TimeCov	0.38	0.02
B	alpha	Gev	0.22	0.02
		MeanDurs	2.91	0.02
		TimeCov	0.38	0.02
	beta	Gev	0.82	0.02
		MeanDurs	0.19	0.14
		TimeCov	0.48	0.02
	delta	Gev	0.60	0.02
		MeanDurs	-2.08	0.02
		TimeCov	-0.49	0.02
	theta	Gev	0.46	0.02
		MeanDurs	0.43	0.02
		TimeCov	0.16	0.48
C	alpha	Gev	0.34	0.02
		MeanDurs	1.50	0.02
		TimeCov	0.16	0.02
	beta	Gev	-1.00	0.02
		MeanDurs	-0.76	0.02
		TimeCov	-1.00	0.02
	delta	Gev	-0.48	0.02
		MeanDurs	-1.64	0.02
		TimeCov	-1.53	0.02
	theta	Gev	-0.50	0.02
		MeanDurs	-0.08	1.00
		TimeCov	-0.83	0.02
C'	alpha	Gev	0.00	1.00
		MeanDurs	2.50	0.02
		TimeCov	0.05	1.00
	beta	Gev	-0.24	0.02
		MeanDurs	-0.20	0.24
		TimeCov	-0.54	0.02
	delta	Gev	1.52	0.02
		MeanDurs	-1.17	0.02
		TimeCov	0.63	0.02
	theta	Gev	0.31	0.02
		MeanDurs	0.31	0.02
		TimeCov	0.07	1.00
D	alpha	Gev	0.02	1.00
		MeanDurs	2.44	0.02
		TimeCov	0.14	0.02
	beta	Gev	-0.40	0.02
		MeanDurs	-0.30	0.02
		TimeCov	-0.73	0.02
	delta	Gev	1.26	0.02
		MeanDurs	-1.47	0.02
		TimeCov	0.17	1.00
	theta	Gev	1.15	0.02
		MeanDurs	0.81	0.02
		TimeCov	0.87	0.02

Table 2: For each between conditions (EO/EC) test P values (p) and cohen's d (d) are reported for all combinations of band, map and metric.